Convective Heat Transfer Coefficients in a Building-Integrated Photovoltaic/Thermal System

Luis M. Candanedo and Andreas Athienitis

Department of Building, Civil and Environmental Engineering, Concordia University
Room EV16.117, 1455 Maisonneuve W., Montréal, Québec, H3G 1M8
Tel. (514)-848-2424, ext. 7080, e-mail: lm_canda@encs.concordia.ca

Abstract

This paper presents an experimental study for the development of convective heat transfer correlations for an open loop air-based building-integrated photovoltaic/thermal (BIPV/T) system. The BIPV/T system absorbs solar energy on the top surface, which includes the photovoltaic panels and generates electricity while also heating air drawn by a variable speed fan through a channel formed by the top roof surface with the photovoltaic modules and an insulated attic layer. The BIPV/T system channel has a length/hydraulic diameter ratio of 38 which is representative of a BIPV/T roof system for 30º-45° tilt angles. The results show significant buoyancy effects (for Rayleigh numbers in the range $2\times10^{10}<Ra<5\times10^{10}$) which enhance the heat transfer. Because of the heating asymmetry in the BIPV/T channel, two Nusselt number correlations are reported: one for the top heated surface, and the other for the bottom surface. For the top heated surface the Nusselt number is in the range 6 to 48 for Reynolds numbers ranging from 250 to 7500. For the bottom insulated surface the Nusselt number is in the range from 22 to 68 for Reynolds numbers ranging from 800 to 7060.

1. Introduction

Building-integrated photovoltaic/thermal (BIPV/T) systems produce thermal and electrical energy while resulting in reduced effective system costs when compared to stand alone PV systems [1]. The BIPV/T system absorbs solar energy on the top surface, which includes the photovoltaic panels, and generates electricity while also heating air flowing in a channel between the top surface and an insulated attic layer (see Figure 1). The PV modules replace cladding or roofing elements of the building envelope. Open loop air-based BIPV/T systems supply solar-heated air that can be used either for ventilation, direct space heating, heating through a heat exchanger or as a source for a

heat pump [2, 3]. Accurate convective heat transfer coefficients (CHTCs) are essential for solving the energy balance equations used for lumped parameter network modeling of these systems (see Figure 2). This is necessary to quantify the thermal and electrical energy production, which in turn provides adequate means for sizing associated equipment, such as heat exchangers and electrical inverters. The PV temperatures obtained by solving the energy balance equations for the PV modules are useful in designing the array layout in order to maximize total energy production. The heat transfer coefficients are also important for the development of control algorithms for control of the airflow [4].

The BIPV/T systems of interest in this paper include a variable speed fan that controls the air flow to produce an air outlet temperature that is suited to the specific desired application such as preheated fresh air, source for a heat pump or a heating application through a heat exchanger (e.g. air-to-water heat exchanger to heat water).

So far researchers and designers have relied on heat transfer correlations developed for similar geometries such as pipes and channels. This approach is not satisfactory due to the inherent complexity of BIPV/T channels, which include heating asymmetry, high aspect ratios, non-constant heat fluxes, non-uniform wall temperatures, non-developed flow conditions and non-uniform cross sections due to structural framing.

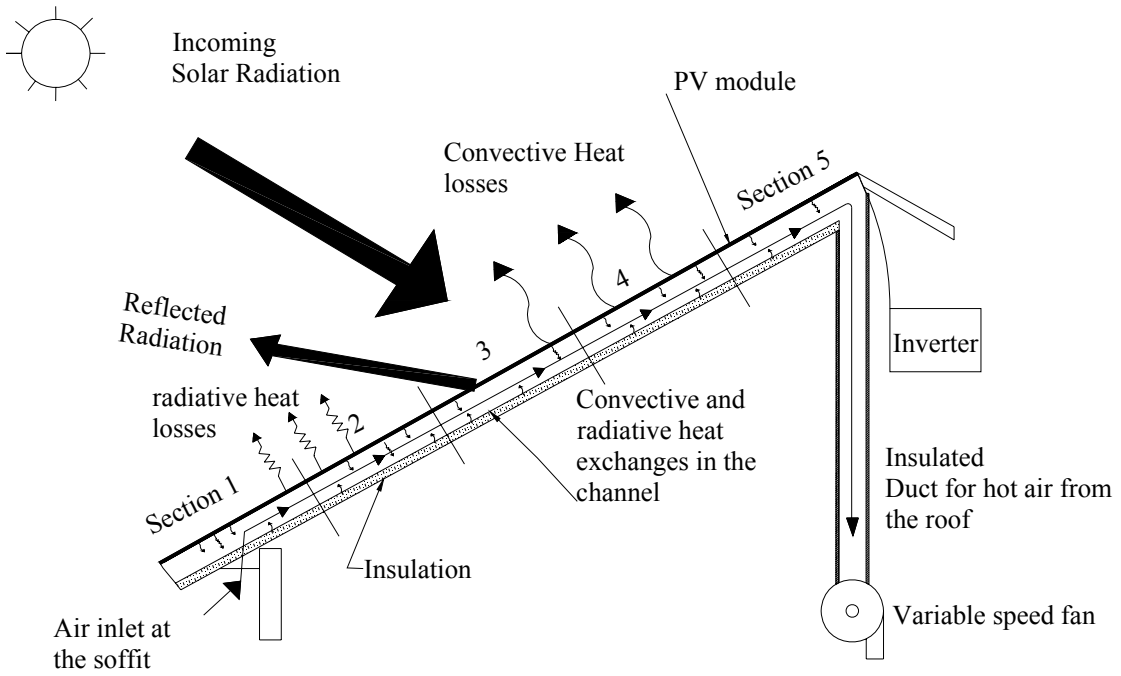

Fig. 1. Schematic of a typical air-based open-loop BIPV/T system [1].

The focus of this work is the determination of the internal convective heat transfer coefficients for a BIPV/T system with outdoor air as the cooling fluid. The channel is smooth and has an aspect ratio (width-to-height) of 10. The channel studied in this paper is smooth in order to obtain the lower limits of the actual heat transfer coefficients.

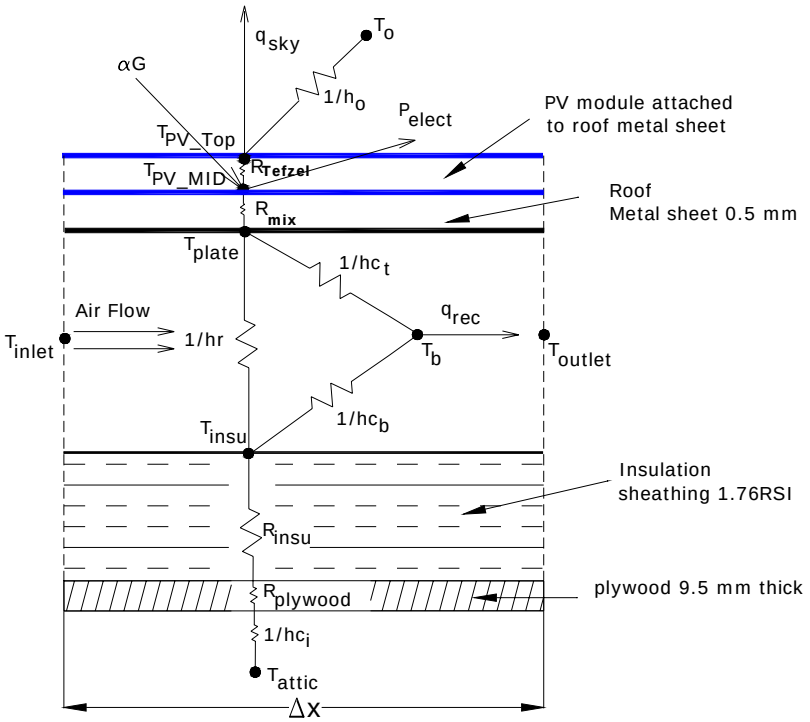

Fig. 2. BIPV/T thermal network model showing the interior convective heat transfer coefficients hc_t and hc_b [1] (the configuration shown corresponds to an experimental prototype studied in this paper).

Figure 2 presents a thermal network schematic of a typical BIPV/T system. For the particular BIPV/T design prototype studied in this paper, an amorphous PV module is mounted on a metal roof sheet. The amorphous PV module is formed from different layers. These are from top to bottom, TEFZEL, antireflective coating, amorphous silicon, a backing substrate, TEFZEL, adhesive and a stainless steel layer to where it was pasted. R_{Tefzel} and R_{mix} represent the thermal resistances of the PV module encapsulant (R_{Tefzel}), the backing substrate and the adhesive combined with the metal roof sheet where it is mounted; hc_t and hc_b represent the convective heat transfer coefficients from the top and bottom surfaces to the bulk air temperature (T_b) node respectively. T_{plate} and T_{ins} represent the temperatures of the plate and the insulation used to compute the radiation heat transfer and convective heat transfer coefficients. R_{ins} is the thermal resistance of the insulation.

1.2 Equations for a Steady State Model

A set of energy balance equations corresponding to the control volume in Figure 2, are written and solved for model comparison with the experimental results. Equations (1-5) correspond respectively to energy balances at the top surface of the PV module, middle of the PV module, interior surface of the metal plate, air node and the surface of the insulation facing the cavity:

$$\frac{T_{PV_{MID}} - T_{PV_{TOP}}}{R_{Tefzel}} - \varepsilon_1 \sigma \left(T^4{}_{PV_{TOP}} - T^4{}_{sky} \right) - \left(T_{PV_{TOP}} - T_o \right) h_o = 0 \tag{1}$$

$$\alpha(\theta) G - P_{elect} - \frac{\left(T_{PV_{MID}} - T_{PV_{TOP}} \right)}{R_{Tefzel}} - \frac{\left(T_{PV_{MID}} - T_{plate} \right)}{R_{Mix}} = 0 \tag{2}$$

$$\frac{\left(T_{PV_{MID}} - T_{plate} \right)}{R_{Mix}} - q_{rad} - \left(T_{plate} - T_b \right) hc_t = 0 \tag{3}$$

$$\left(T_{plate} - T_b \right) hc_t + \left(T_{insu} - T_b \right) hc_b = q_{rec} \tag{4}$$

$$q_{rad} - \left(T_{insu} - T_b \right) hc_b - \frac{T_{insu} - T_{attic}}{R_{ins} + R_{plywood} + \frac{1}{hc_i}} = 0 \tag{5}$$

$$q_{rad} = \sigma F_{plate,insu} \left(\frac{1}{\varepsilon_2} + \frac{1}{\varepsilon_3} - 1 \right)^{-1} \left(T^4{}_{plate} - T^4{}_{insu} \right) \tag{6}$$

$$\eta_{PV} = \eta_{STC} \left(1 - \beta \left(T_{PV_{MID}} - 25°C \right) \right) \tag{7}$$

$$P_{elect} = \eta_{PV} G \tag{8}$$

$$T_{outlet} = T_{inlet} + \frac{A_{CV} q_{rec}}{\dot{m} c_p} \tag{9}$$

$$T_b = \frac{1}{\Delta x} \int_0^{\Delta x} \left(\frac{hc_t T_{plate} + hc_b T_{insu}}{hc_t + hc_b} + e^{-\frac{W_{PV} (hc_t + hc_b)}{\dot{m} c_p} x} \right) dx \tag{10}$$

In the system of equations above, there are ten unknowns: $T_{PV_{TOP}}$, $T_{PV_{MID}}$ T_{plate}, T_{insu}, T_b, q_{rad}, η_{PV}, P_{elect}, T_{outlet} and q_{rec}. The rest of the variables (solar radiation, exterior temperature, mass flow rates, material properties, etc.) are known inputs. Several necessary parameters and variables are calculated as follows:

- The view factor $F_{plate,insu}$ is calculated as a function of geometric parameters [5].
- The absorptance α of the exposed PV surface is corrected as a function of the angle of incidence of beam solar radiation, as described by King *et al.* [6]. The effect of the angle of incidence is significant during the early morning hours and late afternoon hours. For these models, a correction curve developed specifically for the amorphous PV laminate, calculated according to the procedure described by King et al. [6] and available at the Sandia National Laboratories database [7], was used.
- The sky temperature employed to calculate radiative heat losses to the exterior is obtained with the following formula [8] :

$$T_{sky} = T_a \cdot (0.711 + 0.0056 \cdot T_{dp} + 0.000073 \cdot T_{dp}^{\ 2} + 0.013\cos(\pi \cdot t/12)) \quad (11)$$

- The specific heat of air (c_p) has been calculated for the conditions of temperature and relative humidity measured at the inlet of the channel (see equation 21).
- The exterior convective heat transfer correlation is obtained using different correlations to compare their effects into the results. These are the correlations by Test *et al.* [9], Sharples & Charlesworth [10], McAdams [8] as a function of the wind speed in m/s:

$$h_o = 8.55 + 2.56V_{wind} \quad (12)$$

$$h_o = 11.9 + 2.2V_{wind} \quad (13)$$

$$h_o = 5.7 + 3.8V_{wind} \quad (14)$$

- The interior convective heat transfer coefficients (h_{ct} and h_{cb}) are calculated as average values for the entire channel, according to the correlations developed in this paper and presented in section 4.2

1.3 Framing effects

PV modules are usually installed on the roof by means of custom made metallic or wood support framing, such as the one found in the BIPV/T system of the Northern Light Canadian Solar Decathlon 2005 house [11] (see Figure 3). These framing members enhance the heat transfer by increasing turbulence and change the local distribution of the convective heat transfer coefficients as studied in detail by CFD modeling [12].

Fig. 3. Photo of the wood framing structure employed to support the PV modules in the BIPV/T system of Northern Light Canadian Solar Decathlon 2005 house [11].

2. Convective heat transfer coefficients

Several investigations report that typical correlations used to evaluate the heat transfer coefficient underestimate their actual values such as [13-16]. A short discussion of the literature available is presented below for BIPV/T applications and solar air heaters where the air is drawn through the system with a fan. A discussion on mixed convection effects is also presented. Some of the main correlations from the literature are summarized in Table 1. Work on pure natural convection heat transfer in open ended roof top and facade photovoltaic installations is not the focus of this work and is not reviewed. One may refer to the following publications [17-20] for information on passive cooling of PV modules.

2.1 Correlations employed in BIPV/T models

Eicker *et al.* [13] developed a model for a BIPV/T façade system and compared it to experimental data. It was reported that the model data could not fit the experimental results by using simple heat transfer correlations (e.g. parallel plate) to represent the heat

transfer in the gap formed by the PV module and the colder room side glass. The reported heat transfer coefficients for an average air velocity of 0.3 m/s for a gap of 14 cm were 4 to 5 W/m^{2}K for the hot PV side. For the colder glass side the convective heat coefficient was about 3 W/m^{2}K. Although the Reynolds and Nusselt numbers were not reported, using the information provided the estimated Reynolds number is around 4800, and the estimated Nusselt number between 42 to 52 for the hot PV side and 31 for the colder glass side. Bazilian *et al.* [21] developed a numerical model for a photovoltaic heat recovery system. The model compared three different correlations, one for turbulent flow with uniform heat flux, another developed for smooth solar air collectors by Malik and Buelow [22] and the modified Petukhov equation or Gnielinski correlation [8, 23]. Bazilian and Prasad [14] presented another numerical model for a ventilated PV-roof façade for the natural convection case. The authors point out that the model seemed to underestimate the outlet air temperature and overestimate the PV module temperature.

For solar air heaters, Eicker [24] recommends the use of the Petukhov equation for turbulent flow (Re>3100) and the Tan and Charters equation for fully developed turbulent flow [25]. For laminar flow Eicker recommends Nusselt number correlations by Altfeld [26] and Shah and London [27]. For vertical ventilated photovoltaic façades Eicker states that the free convection regime must be taken into account even when the flow is fan-driven. Then, it is recommended that the Nusselt number should be calculated as a weighed valued of the laminar and turbulent portion i.e. $Nu = \sqrt{{Nu_{lam}}^2 + {Nu_{turb}}^2}$.

Bloem [15] developed a numerical model in the simulation program TRNSYS© for a PV façade and points out that the interior convective heat transfer coefficients were underestimated in the model when compared with measurements. There is no indication which Nusselt number correlation was employed for the validation.

Charron & Athienitis [16] used the Gnielinski correlation modified with the Hausen entrance factor [28] to estimate the heat transfer in a BIPV/T double facade. The authors argued that the convective coefficient correlations possibly resulted in an underestimation of the actual heat transfer coefficients by up to 50%. Another important conclusion is that

the recommended limits for the ratio of Gr/Re^2 have to be revised to determine if the flow is driven by natural, mixed, or forced convection. Chen *et al.* [29] modeled a BIPV/T roof system with a correlation for turbulent flow [30]. Candanedo *et al.* [31] employed the Gnielinski correlation for turbulent flow and another correlation for laminar developing heat transfer [32].

2.2 Correlations employed in air hybrid photovoltaic/thermal (PV/T) collector models

Sopian *et al.* [33] employed a Nusselt number correlation for fully developed turbulent flow [8] for asymmetric heating to model a hybrid PV/T heater. Garg & Adhikari [34] employed the Tan and Charters correlation in their numerical model. Hegazy [35] used a Nusselt number correlation that contains an exponential correction to account for the diminishing convective heat transfer away from the entrance [36].

Ong [37] employed different Nusselt number correlations depending on the fluid flow regime. For laminar flow he employed the Heaton correlation, for transitional flow the Hausen correlation, and for fully turbulent flow the Tan and Charters and the Petukhov correlations. The difference between predicted and experimental air temperature predictions was around 5 °C [37].

Ito *et al.* [38] used the Mercer correlation for laminar convection [8]. For forced convection he employed a modified version of the Kays and Crawford correlation which considers the developing flow conditions [8].

2.3 Context of the heat transfer correlations

The previous correlations are valid as long as the conditions for which they were developed are met. A brief description of how the correlations were obtained through experiments is presented below, which identifies under which conditions they would represent the convective heat transfer in a BIPV/T cavity.

Dittus and Boelter [39, 40] developed their correlation for tubes by averaging the results of different researchers. Incropera and DeWitt [5] recommend the use of the Dittus and Boelter equation for Re>10,000 and length to D_h ratios (L/D) > 10. In contrast, McAdams

[41] recommends the Dittus and Boelter equation but in a more restrictive manner for the range 10,000<Re<120,000 and for ratios of L/D of 60 or more. McAdams [41] also recommends the equation for "moderate temperature differences" without giving detail on what can be considered moderate temperature differences.

A correlation that has not been used in BIPV/T systems or in solar air collectors is the Martinelli equation [42]. This equation is recommended in Kakac & Yener [43] for turbulent flow in pipes and for parallel plates. The original paper contains typos in some of the equations. The corrected equations can be found in [41] and a list of the assumptions is given. One of the main features of the Martinelli equation is that it can explain the heat transfer behavior for different Prandtl numbers. It considers the use of the bulk air temperature to determine the heat transfer coefficient and the friction factor.

Tan & Charters [44] studied the effect of the entrance length using a duct with 103 diameters of heated length. The Reynolds numbers ranged from 9500 to 22000. In the report there is no indication that the channel was tilted. The work was further expanded to present a Nusselt number for developed flows [25]. The experimental data showed lower heat transfer rates compared to Dittus-Boelter correlation. Results agree with those obtained by Sparrow for an asymmetrically heated channel [45]. In Sparrow's investigation, the duct had two sections, an initial unheated section with a length of 40 D_h followed by a the heated section with length equal to 140 D_h (in Sparrow's investigation the orientation of the duct was horizontal). A description of the setup can be found in [46].

Cheng & Hong [47] performed a numerical study with inclined tubes at low Reynolds number (5<Re<20). Strong buoyancy effects on heat transfer were found at Rayleigh numbers above 100 for the tilted tube.

Experimental results by Malik & Buelow [48] were obtained using ducts of length 162 D_h. Although not explicitly stated, it appears that the duct was horizontal. Two ducts were analyzed, one with a flat cover and one with a corrugated cover.

2.4 Limitations of the correlations that have been used in BIPV/T modeling

Most of the correlations were developed for high Reynolds numbers (above 10,000), and employed long heated lengths to establish fully developed conditions. Also, most of the studies have been carried out in horizontal channels and pipes where buoyancy effects might not be as strong. Most of them investigated symmetrical heating while in a BIPV/T system it is asymmetric. In a typical roof BIPV/T system, such as the one in EcoTerra™ EQuilibrium demonstration solar house [3], the length of the system is 5.8m. It has an L/D_h ratio of about 70 and it is installed at a 30° tilt angle.

2.5 Mixed Convection Studies

Metais & Eckert [49] presented forced, mixed and free convection regime maps for flow through vertical and horizontal tubes. The objective of their investigation was to determine under which conditions forced or natural convection can be ignored. The authors acknowledged that "the limits between the various flow regimes have to be considered tentative until more experimental results are available".

Petukhov [50] presented equations to establish Grashof numbers when buoyancy effects will affect the heat transfer by about 1% from its value for forced convection, for vertical pipes, and for horizontal pipes. When these limits are surpassed, the actual Nusselt numbers will be at least 1% higher than the values predicted by forced convection correlation for circular pipes. The equations are functions of Reynolds and Prandtl numbers as follows:

For vertical pipes:

$$Gr_q = \frac{1.3\cdot10^{-4}Re^{2.75}Pr\left[Re^{1/8}+2.4\left(Pr^{2/3}-1\right)\right]}{\log(Re)+1.15log(5Pr+1)+0.5Pr-1.8} \quad (15)$$

For horizontal pipes:

$$Gr_q = 3\cdot10^{-5}Re^{2.75}Pr^{0.5}\left[1+2.4\left(Pr^{2/3}-1\right)Re^{-1/8}\right] \quad (16)$$

where, Gr_q

$$Gr_q = \frac{g\beta q_w D^4}{v^2 k} \quad (17)$$

Gnielinski [28] states that there are two main factors that influence the heat transfer coefficient for air, nitrogen, and helium: a) variable physical properties and b) natural convection; variable physical properties for gases do not increase the heat transfer more than 10%; however, the effect of free convection may increase the heat transfer three to four times more than the estimated heat transfer due to pure forced convection alone.

Jackson et al. [51] studied combined free and forced convection in a vertical tube where the tube wall temperature was maintained constant. A Nusselt number correlation was developed. Brown & Gauvin [52] studied combined free and forced convection in aided flow in a vertical pipe (aided or assisted flow occurs when air flows upward in a heated pipe and downward in a cooled pipe). Brown and Gauvin's results show a decrease in Nusselt numbers for assisted laminar flow compared to experimental data presented by Hallman [53] and [54]. However, for turbulent flow, the heat transfer was augmented compared to the equation presented by Hausen [55] for assisted flow. Axcell & Hall [56] carried out experiments for downward flow of air in a vertical pipe for Reynolds numbers between 20,000 to 130,000. For a Reynolds number of 18,800 the measured Nusselt number was 164, which was more than 2.7 times higher than the Nusselt number predicted with the Petukhov and Kirillov equation and 3.1 times higher than the Nusselt number given by the Dittus-Boelter correlation. Axcell & Hall [56] also compared their experimental results against a correlation developed by Fewster & Jackson [57] developed for turbulent buoyancy assisted flow flows and their results were still 20 to 25% higher than what the corrected correlation was predicting.

A study on laminar mixed convection heat transfer for water flow through horizontal parallel plates with asymmetric heating was done by Osborne & Incropera [58]. As expected, it was found that the asymmetric heat flux caused higher Nusselt numbers at the bottom insulated surface than at the top surface.

A comprehensive review of mixed convection in vertical tubes is presented by Jackson *et al.* [59]. They report that for laminar mixed convection regimes in assisted flow convection in vertical tubes, the heat transfer is almost always enhanced. However, for some combinations of $\overline{Gr_b}/Re^{2.7}$ in the turbulent flow mixed convection regime for pipes, the results show that there is a heat transfer drop. For the case of downward buoyancy

opposed flow, the heat transfer is always enhanced. The same type of behavior is reported in a paper by Aicher & Martin [60] on mixed turbulent convection in vertical tubes.

Sudo *et al.* [61] carried out experiments in a vertical duct and explored the effect of aspect ratio on the heat transfer. Results were reported based on dimensional parameters. When $Gr_x/Re_x^{21/8}Pr^{1/2}$ is between 10^{-4} and 10^{-2}, in both aiding and opposing flow, the heat transfer is on average higher than those predicted by correlations. In their paper, the ratio of the measured Nusselt number over the predicted Nusselt number by the Dittus-Boelter correlation is presented. Correlations are also presented based on aiding and opposing flows. In this investigation, most of the time, heat transfer enhancement was found for buoyancy assisted and opposed flows. More recently, Zhang & Dutta [62] studied mixed buoyancy assisted convection with asymmetric heating conditions in a vertical, square channel. The fluid employed was water. It was found that the Nusselt number was higher than predicted with the Gnielinski equation. The Nusselt numbers were also higher when compared to the Nusselt number ratio predicted by the Cotton and Jackson equation [59]. The authors presented a new formula in Dutta *et al.* [63] to correlate Gr/Re with the ratio of the actual Nusselt number to the Nusselt number predicted by Dittus and Boelter.

2.6 Friction factor correlations

Many of the heat transfer correlations employed in the literature have been developed as a function of a friction factor. ASHRAE [64] recommends the use of the friction factor equation developed by Churchill [65]. The advantage of the equation is that it is valid for all ranges of Reynolds numbers (laminar, transitional and turbulent).

The equation is:

$$f = 8\left[\left(\frac{8}{Re_{Dh}}\right)^{12} + \frac{1}{(A+B)^{1.5}}\right]^{1/12} \tag{18}$$

where

$$A = \left[2.457ln\left(\frac{1}{\left(\frac{7}{Re_{Dh}}\right)^{0.9} + \left(0.27\frac{\varepsilon}{Dh}\right)}\right)\right]^{16} \qquad B = \left[\frac{37530}{Re}\right]^{16} \tag{19a, 19b}$$

Table 1.
Nusselt number correlations for flow in a cavity or duct

Author / Reference	Correlation/ Comments	Flow & Heating conditions
Dittus-Boelter [39-41, 66]	$Nu = 0.023Re^{0.8}\mathrm{Pr}^{0.4}$	Average *Nu* for forced convection and symmetrical heating
	Recommended for fully developed turbulent (hydrodynamically and thermally) flow in smooth pipes for Re≥10,000 and L/D≥10 0.7<Pr<160 [5] 10,000>Re>120,000 , L/D>60 and moderate ΔT[41]	
Gnielinski correlation [5]	$Nu = \frac{(Re-1000)Pr\frac{f}{8}}{1+12.7\sqrt{\frac{f}{8}}(Pr^{\frac{2}{3}}-1)}$	Average *Nu* for forced convection and symmetrical heating
	Smooth tubes, For 3000<Re<5×10^6 0.5<Pr<2000	
Modified Petukhov equation for short channel lengths and [24] pipes	$Nu = \frac{(Re-1000)Pr\frac{f}{8}}{1+12.7\sqrt{\frac{f}{8}}(Pr^{\frac{2}{3}}-1)}\left(1+\left(\frac{D_h}{L}\right)^{2/3}\right)$	Average *Nu* for forced convection and symmetrical heating
	Where, $f = (0.79\ln(Re)-1.64)^{-2}$ and Re≥3,000	
Tan and Charters [24] for air (Pr ≈ 0.71)	$Nu = 0.0158Re^{0.8} + (0.00181Re + 2.92)e^{(-0.03795L_c/D_h)}$	Average *Nu* for forced convection and asymmetrical heating
	for a horizontal duct, Re>9500	
Martinelli [41] Note: Original Nu correlation presented in [42] but had typographical errors and was corrected in	$Nu = \frac{Re\cdot Pr\cdot\sqrt{f/2}}{\left(\frac{t_w-t_b}{t_w-t_c}\right)\cdot 5\cdot\left(Pr+ln(1+5Pr)+0.5N_{DR}ln\left(\frac{Re}{60}\sqrt{\frac{f}{2}}\right)\right)}$	Average *Nu* for forced convection and symmetrical heating

[41].	where T_w is the temperature of the wall, T_b the bulk air temperature, and T_c temperature at the center of the pipe. N_{DR} is a diffusivity ratio that depends on Re and Peclet number. N_{DR} is plotted against Re and Pr in [42], for air Pr=0.71 and 1000<Re<10000, 0.7<N_{DR}<0.98. t_w-t_b = Δtmean, t_w-t_c = Δtmax For air $(t_w-t_b)/(t_w-t_c)$ 0.78 to 0.84 for 2000<Re< 10000	
Malik and Bluelow [21]	$$Nu = \frac{0.0192Re^{\frac{3}{4}}Pr}{1 + 1.22Re^{-\frac{1}{8}}(Pr-2)}$$ Recommended for 10000<Re<40000 and L/D_h >162	Average *Nu* for forced convection and asymmetrical heating
Mercer correlation [8]	$$Nu = 4.9 + \frac{0.0606\left(\frac{RePrD_h}{L}\right)^{1.2}}{1 + 0.0909\left(RePr\frac{D_h}{L}\right)^{0.7}Pr^{0.17}}$$ Laminar flow Re<2300	Average *Nu* for forced laminar convection and asymmetric heating

3. Experimental Setup

The experimental setup used in this research consists of a near full-scale BIPV/T system and a similar system without PV panels (just metal roof) connected to an outdoor test facility fully instrumented for air collector testing. The BIPV/T system is a small scale version of the roof BIPV/T system in the EcoTerra^{TM} EQuilibrium demonstration near net-zero energy solar house(see Figure 4) [3] that was also designed by members of the present research team.

Clear days with low wind conditions were selected for the experiments so as to reduce the variability due to wind effects and passing clouds.

Fig. 4. Photo of the BIPV/T roof in the EcoTerra™ House (the amorphous PV modules are attached to a metal roof skin on vertical and horizontal wood framing that also creates the flow channel. (The roof has a length of 5.8 m in the flow direction shown by the arrows).

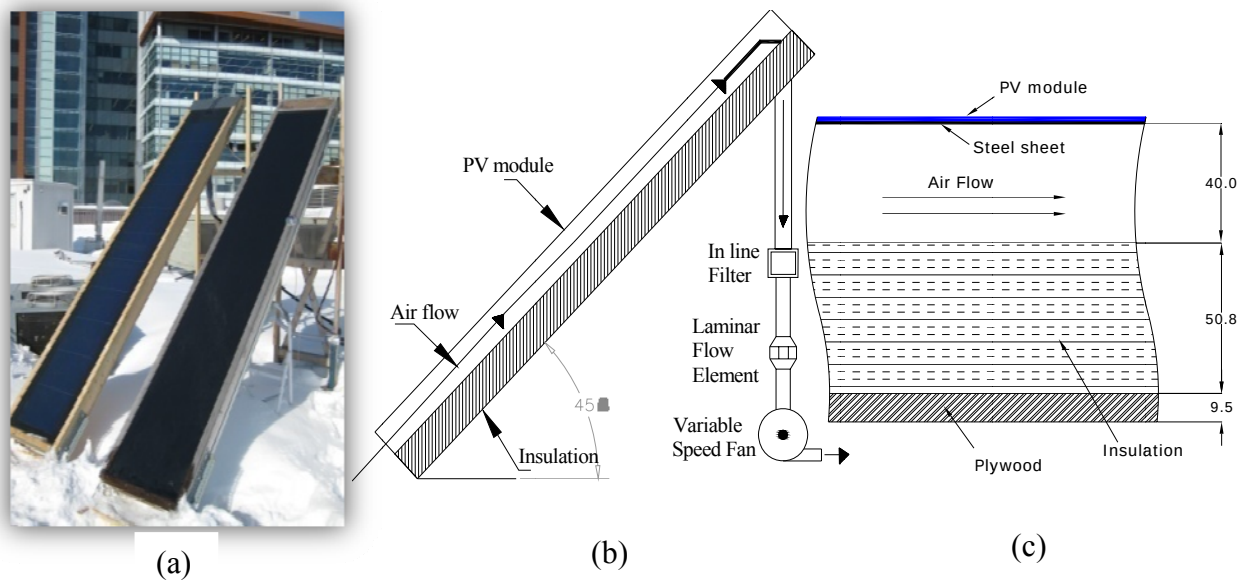

Fig. 5. (a) experimental BIPV/T setup replicating 1 strip of the BIPV/T system of the EcoTerra house with and without amorphous PV modules attached; (b) schematic of the setup; (c) cross section details of BIPV/T.

The solar air collector, (without the PV module) is employed to determine the effect of attaching PV panels on heat generation [1].

The BIPV/T system employs an amorphous PV module with an electrical efficiency of 6% at standard test conditions. This module was attached through built-in adhesive to a steel metal roof sheet with a thickness of 0.5 mm. The cross sectional area of the channel A_c was 0.01549 m^2. The hydraulic diameter D_h is given by $4A_c/U$, where U is the wetted

perimeter (D_h= 0.073 m). The length of the channel was 2.84 m. The thermocouples were special limit T-type with a 0.3°C maximum error. The tilt angle employed in the majority of the experiments was 45°, followed by several tests at a tilt angle of 30º to determine whether natural convection effects had any significant effect in this slope range. The channel considered is smooth with no framing. The bottom of the channel consists of 2 inches of polysterene insulation 1.76 Km^2/W (R-10) and 9.5 mm (3/8 in) thick plywood board (see Figure 5).

Since the major thermal gradients exist along the direction of the flow, 40 thermocouples were placed in the middle of the channel from the inlet to the outlet. Infrared photos of the metal channel showed insignificant thermal variation along the width. The same type of behavior was reported by Ong [37]. The following temperatures were measured: average inlet and outlet air temperature, the temperature of the interior side of the metal plate and the surface temperature of the insulation.

The electrical energy production was recorded every minute by a data acquisition system. The PV module was connected to a charge controller with a maximum power pointtracker. The wind speed and ambient air temperature were recorded by a weather station. The anemometer was a 3-cup type. The wind speed and the ambient air temperature sensors were placed about 10 m above ground.

The total convective heat transfer to the air for each of the control volumes in the BIPV/T cavity was calculated as follows:

$$Qin_{cv} = \dot{m} \cdot c_p \cdot (T_{outlet} - T_{inlet}) \tag{20}$$

T_{outlet} is the average temperature of the air at the outlet and T_{inlet} is the average air temperature at the inlet (may be higher than T_o due to local heating from the ground). The specific heat c_p is given by the equation:

$$c_p = c_{pa} + W \cdot c_{pv} \tag{21}$$

where W is the air moisture content, c_{pa} is the specific heat of dry air and has the value of 1.0 kJ/(kg_a-K) and c_{pv} is the specif heat of water vapor and has the value of 1.86 kJ/(kg_v-K). The moisture content of the air has been calculated using the relative humidity (RH) and the dry bulb temperature. The saturation pressure has been calculated based on correlations provided by ASHRAE [64]. The mass flow rate was measured with a laminar

flow element (LFE). The LFE comes with a calibration curve in order to determine the actual volumetric flow rate. This curve gives the flow rate as a function of the pressure drop across the LFE .

It was found that taking 40 measurements per minute gave a reading that was sufficiently representative for the flow rate calculations. The LFE was calibrated by the manufacturer for a range of 0 to 0.05 m^3/s (0 to 105 CFM). The pressure drop at the maximum flow rate was about 2000 Pa (8 in of water). For this LFE the largest error was 0.25 CFM compared to their calibration standard. The fan can provide a flow rate of up to 0.023 m^3/s (47.5 CFM) with a maximum average velocity of 1.45 m/s through the channel. The pressure transducer used for the LFE can measure pressure from 0 to 2500 Pa (10 inches of water) with 0.25% FS accuracy.

Because of relatively high longitudinal thermal gradients for the metal plate and the insulation along the direction of the flow, the channel was divided into six control volumes. The radiation exchange for a control volume between the interior surface of the metal plate and the insulation surface is given by

$$\mathrm{Qrad}_{cv} = \frac{F_{plate,insu} \cdot A_{cv} \cdot \sigma \cdot (\overline{T^4}_{plate} - \overline{T^4}_{insu})}{\frac{1}{\varepsilon_1} + \frac{1}{\varepsilon_2} - 1} \tag{22}$$

where ε_1 and ε_2 are the longwave emissivities of the surfaces. The emissivities were measured using a calibrated hemispherical emissometer. The measured emissivity of the steel plate was 0.80 while the corresponding value for the insulation board was 0.20. $F_{plate,insu}$ is the view factor between the two cavity surfaces [5].

3. 1 Transient Response

The BIPV/T system would usually reach steady state after 8-9 minutes for approximately constant solar radiation and exterior wind speed as shown in Figure 6.

Kakac [67] studied the effect of step changes in the boundaries of a channel with a numerical analysis; the transient response for Re≈9370 needed approximately 0.07

seconds to reach steady state for the configuration studied. This analysis however does not consider the thermal capacitance and resistance of the materials.

A practical way of analyzing the time response of the system is to consider it a simple RC thermal circuit. The time required to reach 63% of steady state change is the product RC (time constant) where R is the thermal resistance and C the total thermal capacitance; after five time constants, steady state is approximately attained. The combined thermal capacitance of the module and the metal roofing steel sheet was 7838 J/m^{2}K, with a combined thermal resistance of 0.011 m^{2}K/W. The time constant, (RC), was 86.2 seconds. The approximate time to reach steady state (5*RC) is 7.2 minutes. This value is significantly close to the measured value stated above (8-9 minutes).

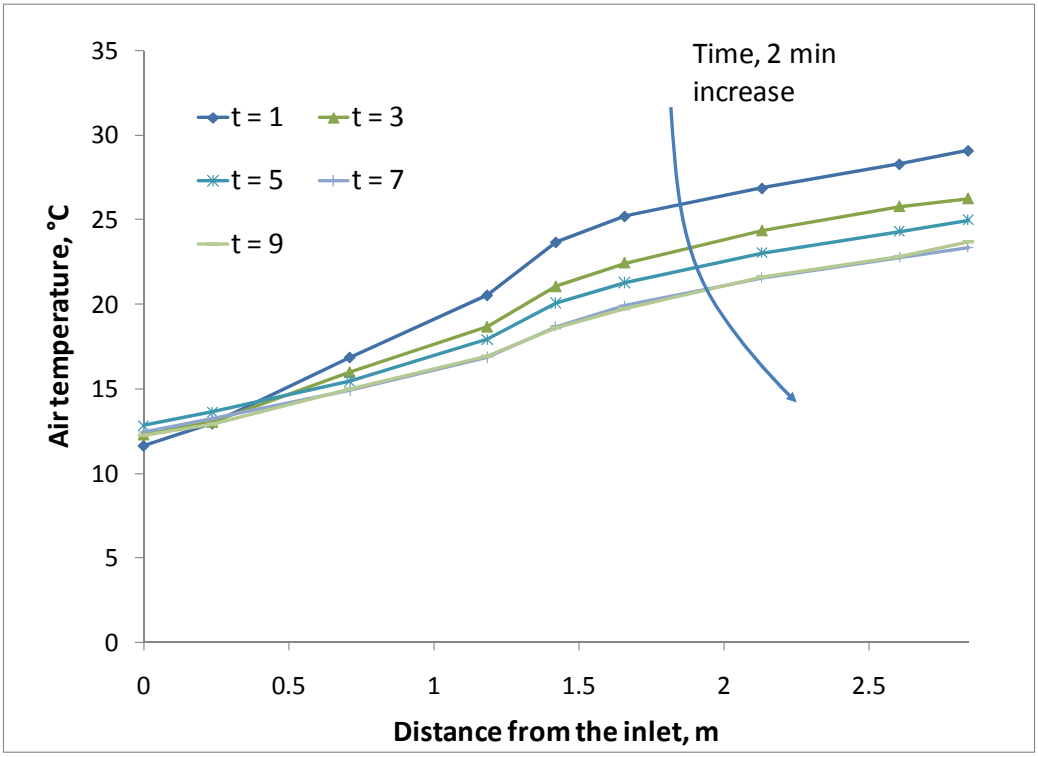

Fig. 6. Transient response of the bulk air temperature for constant volumetric flow rate 0.021m^3/s and incident total solar radiation 815 W/m^2 (the arrow shows increasing time)

The bulk air temperature rise in the channel follows an exponential trend. An exponential correlation was fitted to the experimental data based on an optimized version of the Levenberg-Marquardt method using Mathcad [62]. The equation has the following form

$$T_b(x) = A\left(1 - e^{-\frac{x}{B}}\right) + C \qquad (23)$$

where A, B, and C are fitted parameters. The correlation coefficients (R^2) of the regressions shown in Figure 7 are high ($R^2 \approx 0.99$).

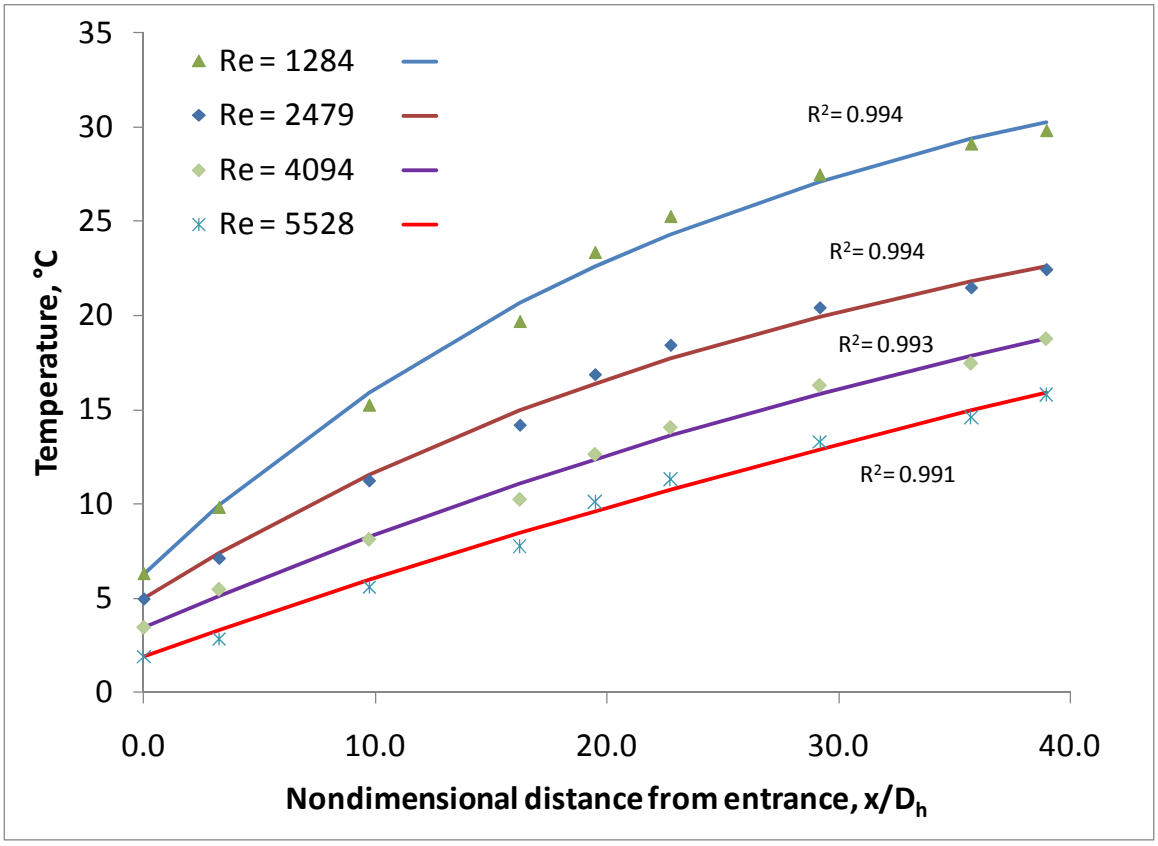

Fig. 7. Bulk Air temperature for different Reynolds numbers compared with exponential correlation fits (points show experimental measurements and solid lines the exponential fit).

3.2 Computation of Convective Heat Transfer Coefficients

Average internal instantaneous CHTC were obtained by using the local averaged temperatures of the PV and the insulation (T_{PV} and T_{ins}) each minute. The air temperature distribution is known from the corresponding exponential formula fitting for the flow rate. Then, local coefficients can be calculated for each control volume. The convective heat transfer coefficient for the corresponding control volume for the top plate was computed as

$$hc_{t,cv} = \frac{Qin_{cv} - Qrad_{cv}}{A_{cv}\left(\overline{T_{plate}}_{cv} - \overline{T}_{b_{cv}}\right)} \tag{24}$$

where Qin_{cv} is determined with equation (20) and $Qrad_{cv}$ was computed with equation (22).

For the bottom surface,

$$hc_{b,cv} = \frac{Qrad_{cv}}{A_{cv}\left(\overline{T}_{insu,cv} - \left(\overline{T}_{b,cv}\right)\right)} \tag{25}$$

In this analysis, the bottom heat loss can be considered negligible due to the comparatively high value of the insulation thermal resistance. This approach of employing two heat transfer coefficient is not new. Two Nusselt numbers, one for each of the control boundaries have been used in parallel plates, channels by [68] [45] [58] and for asymmetric heating in concentric circular tubes [69].

The average Nusselt numbers are in turn given by

$$Nu_{top} = \frac{\overline{hc_t} D_h}{k_{air}} \tag{26}$$

for the top channel surface and by

$$Nu_{bot} = \frac{\overline{hc_b} D_h}{k_{air}} \tag{27}$$

for the bottom surface.

4. Results and Discussion
5.

4.1 Local effects

The local Nusselt numbers are plotted in Figure 8. As can be seen, when the flow is turbulent, it reaches fully developed conditions in shorter lengths. The behavior is opposite for the laminar flow conditions. It is important if fully developed heat transfer condition is reached in order to decide whether a local or an average heat transfer coefficients can be used.

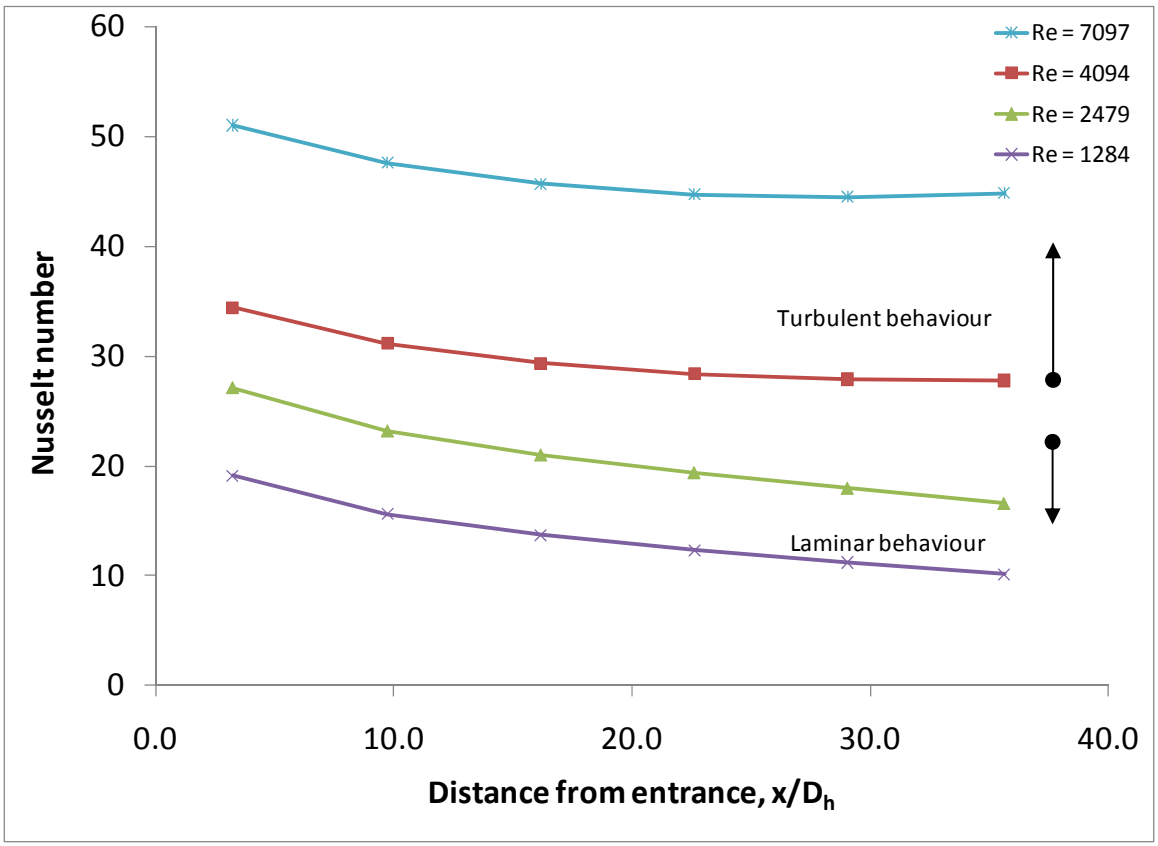

Fig. 8. Local Nusselt number for the top surface versus non dimensional distance from the entrance.

Many researchers have studied Nusselt number developing length solutions for laminar and turbulent flow. To obtain the fully developed solution for the laminar flow (Re<2300) Kays [69] recommends for the entry length solution for the circular tube the relationship

$$\frac{x}{D_h} \approx 0.05RePr \tag{28}$$

while Hallman [53] employs the relationship

$$\frac{x}{D_h} > 0.0425RePr \tag{29}$$

However, for the turbulent region, White [70] states that the developing length is shorter and it can be estimated with

$$\frac{x}{D_h} \approx 4.4Re^{1/6} \tag{30}$$

The experimental results agree with the previous correlations to determine the developing length. For instance at Re ≈ 1284, the developed flow conditions are reached when x/D_h ≧ 38.7 based on equation (29). Comparing this result to Figure 8, where for $x/D_h = 29$ to $x/D_h = 36$ the change in Nusselt number is about 9.6%, clearly not being fully developed yet. However, in the turbulent region, for Re ≈ 4094 the developed flow conditions are reached when x/D_h ≧ 17.6 based on equation (30). The experimental data suggest that for an increase of x/D_h from 16.2 to x/D_h=22.6, the Nusselt number decrease is only 3%.

4.2 Average Nusselt Numbers

The average Nusselt number coefficients for the top and the bottom surfaces were calculated from the local distributions and graphed as a function of the Reynolds number in Figures 9 and 10. Since the inlet air temperature is not controlled, Nusselt number data for other Rayleigh numbers cannot be studied. Because of that, a correlation for the average Nusselt number as a function of the Reynolds number has been obtained. It was found by means of an optimized version of the Levenberg-Marquardt method for minimization [71].

For the top surface, for 250 ≤ Re ≤ 7500

$$Nu_{top} = 0.052Re^{0.78}Pr^{0.4} \quad (31)$$

and for the bottom surface, for 800 ≤ Re ≤ 7100

$$Nu_{bottom} = 1.017Re^{0.471}Pr^{0.4} \quad (32)$$

The correlations along with the uncertainty in the data are plotted in Figures 9 and 10. The appendix summarizes how the uncertainties were calculated. As can be seen, the Nusselt numbers for the bottom surface are higher than the ones for the top surface. Sparrow *et al.* [45] found the same behavior in the experiments where the heated wall has a lower Nusselt number than the unheated one. In the present case, because the bottom surface is insulated, the heat gain by longwave radiation from the top heated surface is approximately equal to the heat transfer to the air by convection, thus resulting in a small temperature differential between the bottom surface and the air.

The uncertainties in the Nusselt number for the top surface are very small. In general, they range between 4.8% to a maximum of 7% for 1760<Re<7500. The highest

uncertainties occur at the lowest Reynolds numbers. For example, the uncertainty is 66% at Re = 256 and 13% for Re = 802. The same behavior has been reported by Novotny *et al* [46]. The uncertainties for the Re numbers are between 3.3 to 8% for 1100<Re<7500. At low flow rates the uncertainties are higher, e.g. for Re = 250 the uncertainty is 31% and for Re = 800 is 10%.

The experimental results show significantly more uncertainty regarding the heat transfer coefficients of the bottom surface; however, their effect on outlet air temperature calculation is far less important than that of the heat transfer coefficients of the top heated surface. The high uncertainties are due to the fact that the air bulk temperature and the surface temperature are very close so that small error in the temperature measurement can cause high errors in the heat transfer coefficient. Barrow [72] obtained similar scattered results in the data because of high uncertainty in the Nusselt number.

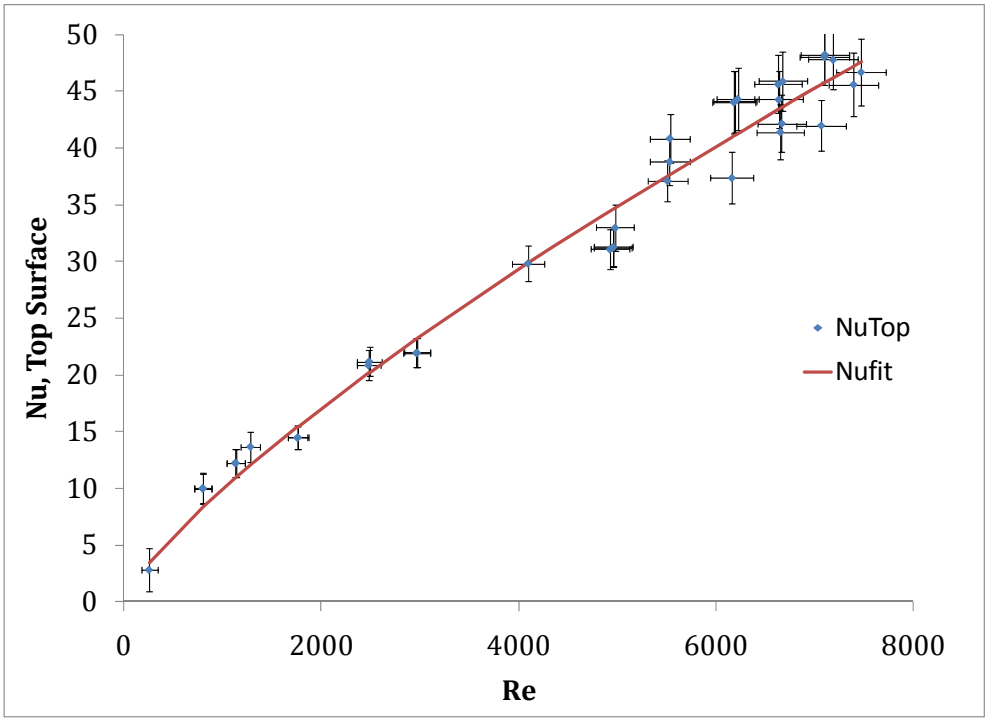

Fig. 9. Nusselt numbers for the top surface versus Reynolds number. The data is compared with the correlation given by equation 18. (The uncertainties of each of the data points are shown by the vertical line segments).

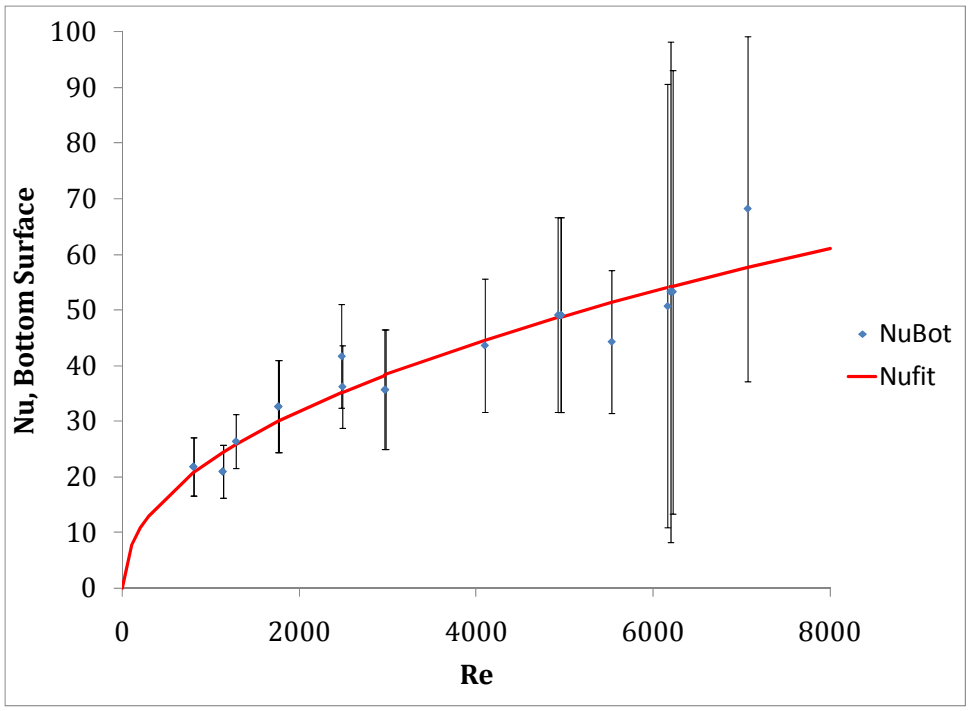

Fig. 10. Nusselt numbers for the bottom surface versus Reynolds number. The data is compared with the correlation equation 19. The uncertainties of each of the data points areshown by the vertical bars.

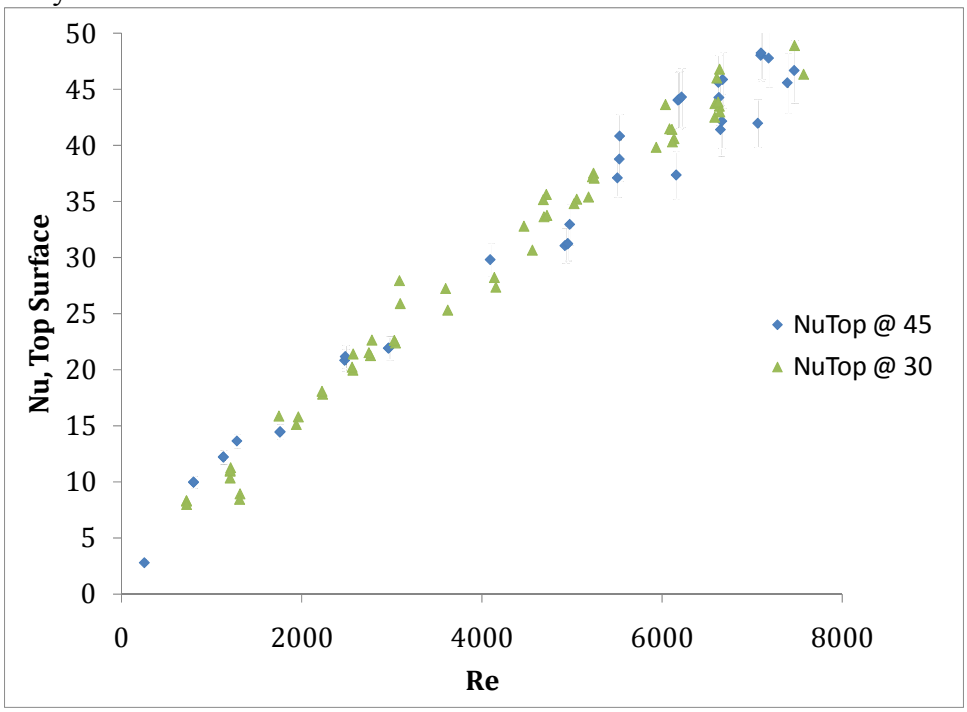

Fig. 11. Nusselt numbers for the top surface versus Reynolds number comparison for 45º and 30º tilt angles.

The experiment was performed for the tilt angles 30º and 45º since this range represents most Canadian sloped roof housing. The results show no significant difference between 30º and 45º for the Nusselt numbers, except for low Reynolds numbers up to about 1600 where stronger buoyancy effects (due to the steeper angle) are evident. Nevertheless, for the correlations developed, this effect was not considered significant enough to represent for modeling and design purposes.

4.3 Comparison of the new correlation with previous results

The Nusselt numbers for the top surface are compared with a few of the most typical correlations in Figure 12. The Martinelli and Gnielinski correlations were evaluated with the friction coefficient proposed by Churchill [65].

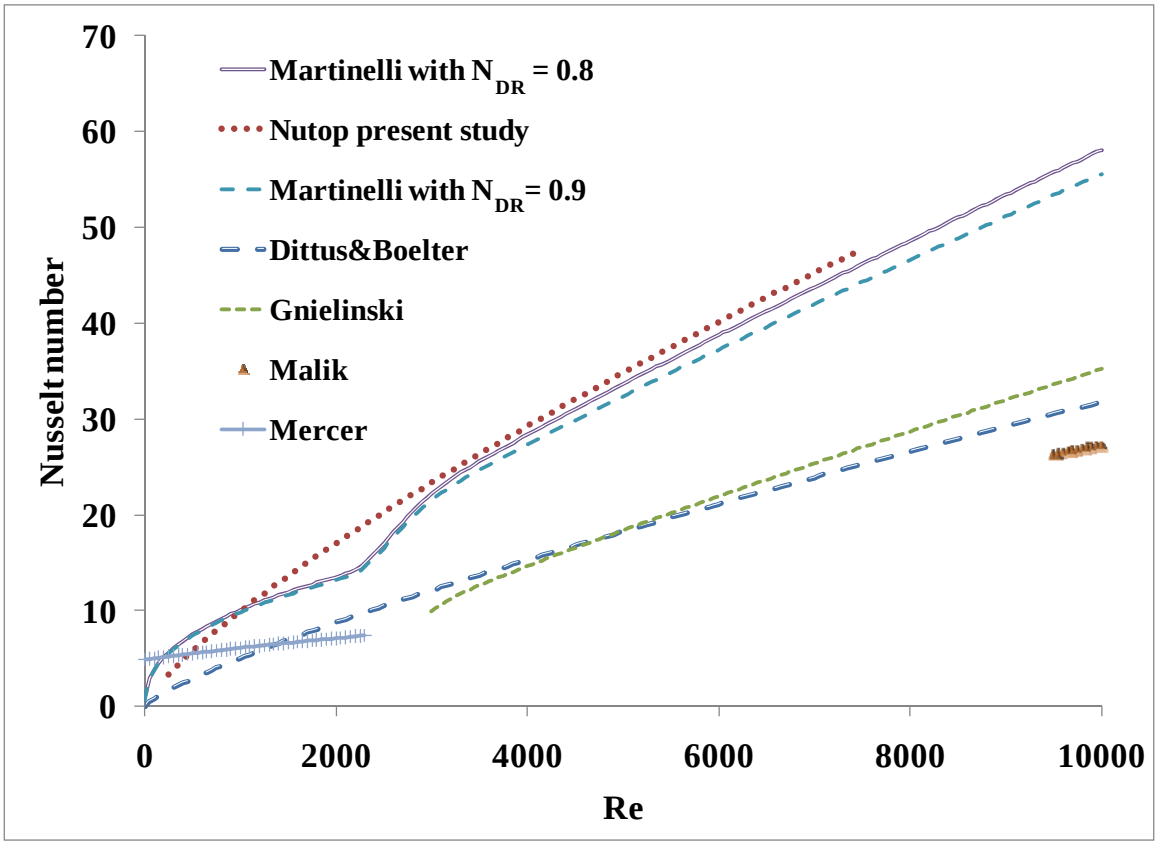

Fig. 12. Comparison of the top channel surface Nusselt number correlation with Dittus-Boelter, Gnielinski, Martinelli, Malik and Mercer correlations.

Although the Dittus-Boelter correlation is recommended for Re> 10,000, it has been plotted to indicate the possible low limit of the heat transfer. As can be seen from Figure

10, the Dittus-Boelter and Gnielinski correlations predict very similar values. Martinelli's correlation includes a correction for the ratio of temperature difference of the wall, the bulk air temperature and the temperature at the center of the duct. The ratio $(T_w-T_b)/(T_w-T_c)$ was computed from the experimental data and ranges from 0.9 to 0.96. Martinelli's correlation predicts the measured Nusselt number for the top surface very close to the current correlation. The experiment, in general, shows higher values of Nusselt numbers in the low Reynolds number range compared to the Mercer correlation and this is mainly due to the fact that fully developed conditions are not attained.

4.4 Grashof and Rayleigh numbers

Petukhov [50] pointed out that when Grashof numbers surpass a certain upper limit, actual Nusselt numbers will be at least 1% higher than the value predicted by forced convection correlations for circular pipes. This "maximum" Grashof number is a function of the Reynolds number (Figure 13), and is different for vertical and horizontal pipes. As can be seen in Figure 13, the Grashof numbers experimentally measured in the BIPV/T channel exceed by several orders of magnitude Petukhov's upper limit curves given by equations 15 and 16. This indicates that forced convection correlations commonly used for circular pipes will be inadequate for the cases discussed in this paper, in which natural convection effects will clearly play an important role.

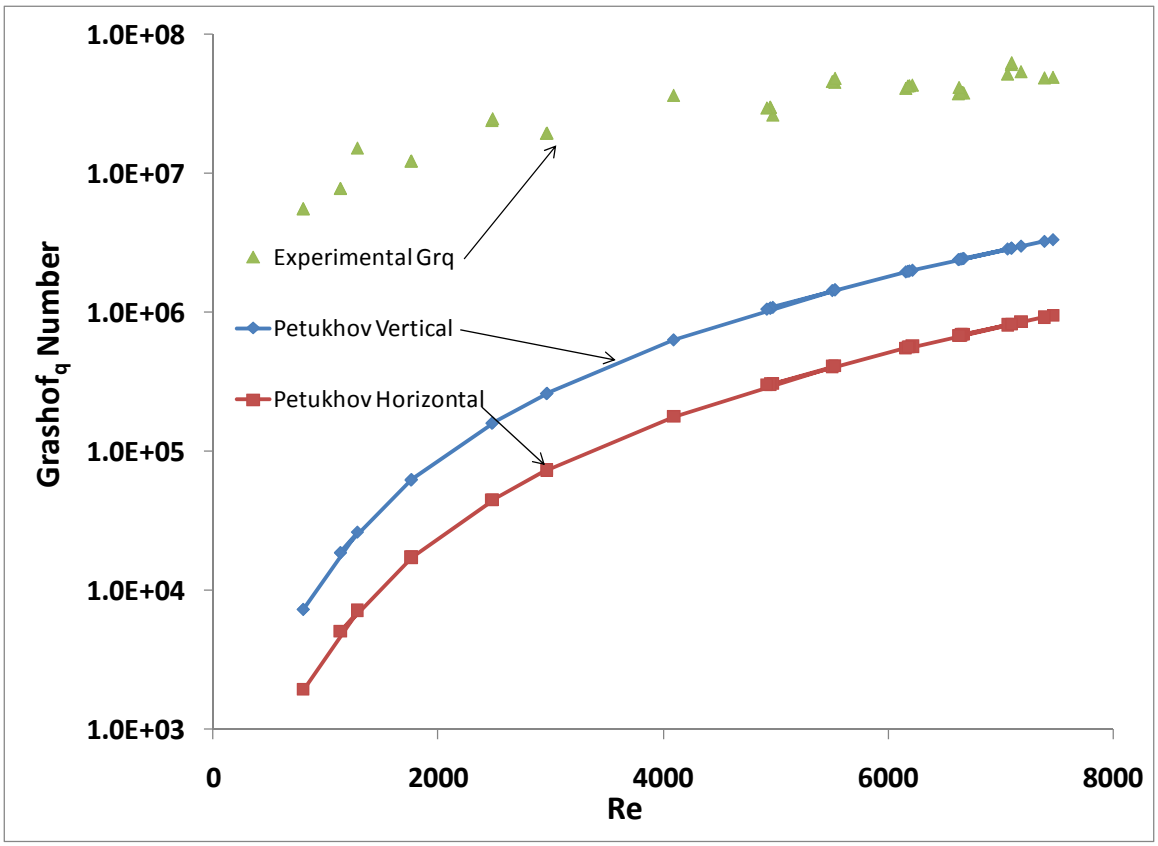

Fig. 13. Comparison of Equations (1) and (2) with the experimental data (Pr=0.71). All the experimental points are above the limits established by the equations.

The experimental data can be compared to the Metais & Eckert maps [49]. Most of the experimental data falls in the mixed regime of turbulent heat transfer ($2\times10^{10}<Ra<5\times10^{10}$). The experimental data are also in agreement with the results obtained by Sudo *et al.* [61] for a vertical heated rectangular channel, for which the Nusselt number is 1.7 to 2.4 times the value predicted by the Dittus-Boelter correlation.

4.5 Numerical sensitivity study of bottom heat transfer coefficient.

Nusselt numbers for the bottom channel surface have a higher uncertainty and it is important to assess the impact of this on the BIPV/T performance. However, because the bottom surface is highly insulated and is not subjected to direct solar radiation, the associated uncertainty is not as critical for the quantitative evaluation of the BIPV/T system. In order to study this question, a validated numerical BIPV/T model as described

in detail in [1] is employed to assess the sensitivity of the bottom heat transfer coefficient to the outlet temperature. The numerical model solves the system of equations presented in section 1.2. Some model input parameters are listed below:

- Inlet air temperature = -5°C
- 5 m long BIPV/T system
- Normal incident solar radiation = 1000 W/m^2
- h_o = 10 W/m^2K
- Flow rate = $8.91\times10^{-3} m^3/s$
- Re = 3000
- D_h = 0.074 m
- hc_t is 7.89 W/m^2K and hc_b is 13 W/m^2K (from equations (31) and (32)),
- Exposed area to solar radiation = $1.94m^2$
- Longwave emissivity of insulation and metal facing cavity equal to 0.2 and 0.8 respectively.

As a result of employing the parameters above in the numerical model, the final predicted outlet air temperature is 26.92°C. If the value of hc_b was forced to be 1.5 times more while keeping all the other parameters constant, the final outlet air temperature would be 26.91°C. This represents only a 0.01°C deviation from the first result or less than 1% error. If the hc_b was forced to be 3 times more, the final outlet air temperature would be 26.84°C. The deviation is now only 0.1°C, or less than 1% error in the final computation of outlet air temperature. Therefore, it can be concluded that the bottom Nusselt number uncertainty is not as important for the determination of the BIPV/T system performance.

5. Conclusion

Experimental measurements of forced convective heat transfer coefficients have been carried out for an open loop BIPV/T system. The BIPV/T system channel had a length/hydraulic diameter ratio of 38 and was tested for 30-45° tilt angles. The data show no significant difference in Nusselt numbers for the 30° and 45° tilt angles, indicating

that buoyancy effects are approximately constant in this range of roof tilt angles that represents the majority of Canadian housing.

Because of the heating asymmetry in the BIPV/T system, two Nusselt number correlations were recommended at different Reynolds number ranges. However, because the bottom surface (near adiabatic) does not contribute significantly to the amount of heat that is added to the air, the associated uncertainty in the correlation is not as critical in calculating the heat recovery by the flowing air and its outlet temperature.

It was found that the Nusselt numbers for the top surface in the present study are significantly higher than the values predicted by the forced convection correlations given by Dittus and Boelter, Gnielinski, and Petukhov [5, 40]. Many of the experimental studies were performed for very long and horizontal channels, and high Reynolds numbers, where buoyancy effects are minimal. The present results also confirm findings by other researchers [13-16] that the Nusselt numbers were underestimated. The Martinelli equation has the best agreement with the present experimental data. This is due to the fact that the equation takes into account the temperature difference between the wall surface and the bulk air temperature.

Correlations (31) and (32) developed in this study are recommended for the determination of the Nusselt number for open loop BIPV/T systems and solar air heaters for tilt angles between 30º and 45º. Currently, investigation of framing effects on Nusselt numbers is being done and it has been found that the framing may increase the actual Nusselt numbers by about 20% due to increased turbulence.

Nomenclature

A	=	collector exposed area, m^2
A_c	=	cross sectional area, m^2
A_{cv}	=	area of the control volume, m^2
b	=	conditions at bulk temperature
c_p	=	specific heat capacity of the air, J/kg·K
d	=	tube diameter, m
D_h	=	hydraulic diameter of the cavity, m
E_p	=	electric power, W
f	=	friction factor
$F_{plate,insu}$	=	view factor between plate and insulation
F_e	=	emissivity factor, $1/(1/\varepsilon_2 + 1/\varepsilon_3 - 1)$

G	=	total incident solar radiation, W/m^2
g	=	gravitational acceleration, m/s^2
Gr	=	Grashof number, $g\,\beta(T_w-T_{bulk})D_h^3/\upsilon^2$
Gr_x	=	Grashof number based on inlet $_{distance}$, $x^3 g\beta(T_w-T_{bulk})/\upsilon^2$
$\overline{Gr_b}$	=	Grashof number, $(\rho_b-\bar{\rho})d^3g/\rho_b^2$
Gr_q	=	Grashof number based on heat flux q_w, $(g\beta q_w D_h^4)/(\upsilon^2 k)$
hc_b,hc_t	=	convective heat transfer coefficient in cavity, $W/m^2\cdot K$
hc_i	=	convective heat transfer coefficient in attic, $W/m^2\cdot K$
h_o, h_w	=	exterior/wind convective heat transfer coefficient, $W/m^2\cdot K$
h_{ro}	=	exterior radiative heat transfer coefficient, $W/m^2\cdot K$
h_r	=	cavity radiative heat transfer coefficient, $W/m^2\cdot K$
k	=	thermal conductivity, $W/m\cdot K$
L	=	length of the channel, m
m	=	average mass flow rate, kg/s
N_u	=	Nusselt number, hD_h/k
N_{DR}	=	diffusivity ratio
Pe	=	Peclet number, $RePr$
P_{elect}	=	electrical power per unit area, W/m^2
Pr	=	Prandlt number, ν/α
$Qrad_{cv}$	=	radiative heat transfer rate in control volume, W
Qin_{cv}	=	convective heat transfer rate in control volume, W
q_{rad}	=	radiative heat exchange between cavity surfaces per unit area, W/m^2
q_{rec}	=	heat recovered in the control volume per unit area, W/m^2
q_w	=	heat flux on the wall, W/m^2
Ra	=	Rayleigh number, $GrPr = g\rho^2 c_p\,\beta(T_w-T_{bulk})D_h^3/(\mu k) = g\,\beta(T_w-T_{bulk})D_h^3/\upsilon\alpha$
Re	=	Reynolds number, $\rho VD_h/\mu$
Re_x	=	Reynolds number based on inlet distance, $\rho Vx/\mu$
R_{Tefzel}	=	Tefzel R value, m^2K/W
R_{insu}	=	insulation R value, m^2K/W
$R_{plywood}$	=	plywood layer R value, m^2K/W
R_{mix}	=	combined thermal resistance, m^2K/W
t	=	time from midnight, h
T_o, T_a	=	exterior air temperature, °C
T_{plate}	=	interior side temperature of the metal sheet, °C, or in K for radiative heat transfer computation
T_{insu}	=	interior side temperature of the insulation, °C, or in K for radiative heat transfer computation
T_{PVMID}	=	temperature of the PV module at midpoint, °C
T_{PVTOP}	=	temperature of the PV module at its external surface, °C
T_{dp}	=	dew point temperature, °C
T_b	=	air bulk temperature in the control volume, °C
T_{sky}	=	sky temperature, K
T_{inlet}	=	inlet air temperature, °C
T_{outlet}	=	outlet air temperature, °C
U	=	wetted perimeter, m
V	=	average air velocity in the channel, m/s

V_w	=	average wind velocity, m/s
W	=	air moisture content, kg_v/kg_a
W_{PV}	=	width of the control volume, m
x	=	distance from inlet of flow channel, m
Greek Letters		
α	=	solar absorptivity
Δx	=	length of the control volume, m
β	=	thermal expansion coefficient, 1/T or PV module temperature coefficient, ($\%K^{-1}$)
ε_1, ε_2, ε_3	=	longwave emissivities
μ	=	dynamic or absolute viscosity, kg/(m·s)
υ	=	kinematic viscosity, m^2/s
θ	=	incidence angle, degrees
φ	=	tilt angle, degrees
α	=	thermal diffusivity, $k/\rho c_p$
σ	=	Stefan Boltzmann constant, W/m^2K^4
ρ	=	air density, kg/m^3
$\bar{\rho}$	=	average air density $1/(T_w-T_b) \iint_{T_b}^{T_w} \rho dT$, kg/m^3
η_e	=	electrical efficiency
η_{PV}	=	electrical efficiency of the PV module
η_{STC}	=	electrical efficiency at standard test conditions
Acronyms		
BIPV/T		building integrated photovoltaic/thermal
CHTC		convective heat transfer coefficient
CFM		cubic feet per minute, ft^3/min
FS		full span
LFE		laminar flow element

Appendix: Measurement Uncertainties

The uncertainties associated with the average Nusselt numbers have been calculated with the propagation rules [73, 74].

Uncertainty in collector area

The exposed collector area was measured with an accuracy of 0.000794 m (1/32in).

The associated error is calculated as

$$\Delta A = 1.1019 \sqrt{\left(\frac{0.000794}{2.84728}\right)^2 + \left(\frac{0.000794}{0.387}\right)^2} = 2.282 \times 10^{-3} m^2$$

For the area A_{cv}, the associated error is then

$$\Delta A_{cv} = \frac{1.1019}{6} * \sqrt{\left(\frac{2.282 \times 10^{-3}}{1.1019}\right)^2} = 3.8 \times 10^{-4} m^2$$

Uncertainty in radiative heat transfer rate

First, the errors associated with the radiative heat transfer rate (equation 22) are calculated based on the uncertainties in the measurement of the surface emissivities of the insulation and metal plate surfaces, together with the errors in the temperature measurement of the surfaces and the associated error in the control volume area. The uncertainty in each of the measured emissivities is 0.3%. The emissivity factor $F_{\varepsilon,}$ and its uncertainty, ΔF_{ε}, is calculated with

$$F_{\varepsilon} \pm \Delta F_{\varepsilon} = \frac{1}{\frac{1}{0.2\pm0.3\%}+\frac{1}{0.82\pm0.3\%}-1} = \frac{1}{5\pm0.015+1.219\pm3.65\times10^{-3}-1} = \frac{1}{5.2195\pm0.01543} = 0.19158 \pm 0.19158\left(\frac{0.01543}{5.2195}\right)$$

and ΔF_{ε} has a value of 5.6×10^{-4}.

The error associated with equation 22, has been calculated by first computing the error in each of the six control volumes associated with the emissivity, the plate temperatures and the area, and finally adding them to compute the total error in the total $\Delta Qrad_{cv}$. i.e.

$$\Delta_{\mathrm{Qradcv}(\Delta T)} = \sigma F_{plate,insu} \mathrm{F}_{\varepsilon} \mathrm{A}_{\mathrm{cv}} \sqrt{((4 * 0.3 * (T_{plate} + 273.15)^3)^2 + (4 * 0.3 * (T_{insu} + 273.15)^3)^2}$$

$$\Delta_{\mathrm{Qradcv}(\Delta\varepsilon)} = \sigma F_{plate,insu} \mathrm{A}_{\mathrm{cv}} \sqrt{(T_{plate} + 273.15)^4 - (T_{insu} + 273.15)^4} * 5.6 \times 10^{-4}$$

$$\Delta_{\mathrm{Qradcv}(\Delta\mathrm{Acv})} = \sigma F_{plate,insu} \mathrm{F}_{\varepsilon} \sqrt{(T_{plate} + 273.15)^4 - (T_{insu} + 273.15)^4} * 3.8 \times 10^{-4}$$

$$\Delta_{\mathrm{Qrad}} = \sqrt{\sum_{\mathrm{n}=1}^{6} \left(\Delta_{\mathrm{Qradcv}(\Delta T),\mathrm{n}}\right)^2 + \sum_{\mathrm{n}=1}^{6} \left(\Delta_{\mathrm{Qradcv}(\Delta\varepsilon),\mathrm{n}}\right)^2 + \sum_{\mathrm{n}=1}^{6} \left(\Delta_{\mathrm{Qradcv}(\Delta\mathrm{Acv}),\mathrm{n}}\right)^2}$$

The uncertainties calculated are in the range of 1.2% of the total Q_{rad}

Uncertainty in convective heat transfer rate

The uncertainties in the convective heat transfer rate arise from measurement uncertainties in different parameters. There are uncertainties in the mass flow rate due to the pressure transducer and the LFE calibration curve, and to uncertainties in the T_{oulet} and T_{inlet} air temperature measurements.

The highest uncertainty for the flow rate is 0.25 CFM due to the calibration curve fitting according to the manufacturer's data of the LFE. The pressure transducer has an accuracy of 6.25 Pa (0.025 in). Then, the ΔCFM has been calculated as

$$\Delta CFM = \sqrt{\left(1.39297 \times 10^{1} \cdot 0.025\right)^2 + 2\left(\frac{2 \cdot 0.025 \Delta P^2}{\Delta P}\right)^2} + 0.25\mathrm{CFM}$$

The maximum ΔCFM is 0.6357 CFM ($3\times10\text{-}4 m^3/s$) due to the combined effects of the error of the calibration curve and the uncertainty in the pressure drop measurement. The ΔT is

the result of the addition of the uncertainties of T_{outlet} and T_{inlet}. The uncertainty in the thermocouples is 0.3°C, then $\Delta T=\sqrt{0.3^2+0.3^2}=0.424°C$.

The maximum uncertainty in the calculation of c_p of air is 0.01% due to error in the measurement of RH (3%). The estimated error associated to density of air is 0.25% [75]. Then, the total uncertainty in ΔQin_{cv} is calculated as:

$$\Delta Qin = \dot{m}c_p(T_{outlet}-T_{inlet})\sqrt{\left(\frac{\Delta T}{(T_{outlet}-T_{inlet})}\right)^2+\left(\frac{\Delta CFM\cdot \dot{m}c_p}{\dot{m}c_p}\right)^2+\left(\frac{\Delta c_p}{c_p}\right)^2+\left(\frac{\Delta\rho}{\rho}\right)^2}$$

Uncertainty in convective coefficient

To obtain the top heat transfer coefficient uncertainty, it is necessary to calculate the uncertainty of Qin-Qrad. Then

$$\Delta_{(Qin-Qrad)}=\sqrt{\Delta Qin^2+\Delta Qrad^2}$$

From equation 24, it follows that the uncertainty in hc_t must consider the uncertainties in the area measurement and in the temperature differential

$$\Delta hc_t = hc\sqrt{\left(\frac{\Delta_{A\Delta T}}{A\Delta T}\right)^2+\left(\frac{\Delta_{Qin-Qrad}}{Qin-Qrad}\right)^2}$$

The uncertainties for hc_b have been calculated in a similar fashion.

Uncertainties in Nusselt numbers

From equation 26, it follows the uncertainty in Nu_{top} is calculated as

$$\Delta Nu_{top} = Nu_{top}\sqrt{\left(\frac{\Delta k_{air}}{k_{air}}\right)^2+\left(\frac{\Delta hc_t D_h}{hc_t t D_h}\right)^2}$$

The uncertainty in k_{air} has been calculated with the Sutherland-law thermal conductivity with the constant provided in [76]. The uncertainty of k_{air} is 2%.

The uncertainties for Nu_{bot} have been calculated in a similar fashion.

Uncertainties in Reynolds Numbers

In order to compute the uncertainties in Re ($\rho VD_h/\mu$), the uncertainties on each of the parameters have been taken into account.

$$\Delta \mathrm{Re} = \mathrm{Re}\sqrt{\left(\frac{\Delta\rho}{\rho}\right)^2+\left(\frac{\Delta V}{V}\right)^2+\left(\frac{\Delta D_h}{D_h}\right)^2+\left(\frac{\Delta\mu}{\mu}\right)^2}$$

The uncertainty in μ has been calculated with the Sutherland-law viscosity with the constants provided in [76]. The uncertainty of μ is 2%.

Acknowledgements

This work was funded by the Canadian Solar Buildings Research Network, a strategic NSERC research network and NRCan-CanmetENERGY (Varennes). The technical assistance of Joseph Hrib and Kwang Wook Park in the set up of the experiment is gratefully acknowledged.

References

1. Candanedo, L.M., A.K. Athienitis, J. Candanedo, W. O'Brien, and Y.-X. Chen, *Transient and steady state models for open-loop air-based BIPV/T systems.* ASHRAE transactions, 2010.
2. Candanedo, J. and A.K. Athienitis. *Simulation of the performance of a BIPV/T system coupled to a heat pump in a residential heating application*. in *9th International IEA Heat Pump Conference*. 2008. Zurich, Switzerland.
3. Chen, Y., A.K. Athienitis, K.E. Galal, and Y. Poissant. *Design and Simulation for a Solar House with Building Integrated Photovoltaic-Thermal System and Thermal Storage*. in *ISES Solar World Congress, Beijing, China*. 2007.
4. Candanedo, J.A., *Investigation of anticipatory control strategies in a net-zero energy solar house.* ASHRAE transactions, 2010.
5. Incropera, F.P. and D.P. De Witt, *Fundamentals of heat and mass transfer*. Fifth ed. 2002: John Wiley & Sons. 981.
6. King, D.L., J.A. Kratochvil, and W.E. Boyson. *Measuring solar spectral and angle-of-Incidence effects on photovoltaic modules and solar irradiance sensors*. in *26th IEEE Photovoltaic Specialists Conference*. 1997. Anaheim, California.
7. Sandia National Laboratories, *Database of Photovoltaic Module Performance Parameters*. 2006.
8. Duffie, J.A. and W.A. Beckman, *Solar engineering of thermal processes*. Third ed. 2006, Hoboken: John Willey & Sons, Inc. 908.
9. Test, F.L., R.C. Lessmann, and A. Johary, *Heat transfer during wind flow over rectangular bodies in the natural environmental.* . Transactions of the ASME J. Heat transfer, 1981. **103**: p. 262-267.
10. Sharples, S. and P.S. Charlesworth, *Full-scale measurements of wind-induced convective heat transfer from a roof-mounted flat plate solar collector.* Solar Energy, 1998. **62**(2): p. 69-77.
11. Pasini, M. and A.K. Athienitis, *Systems Design of the Canadian Solar Decathlon House.* ASHRAE Transactions 2006. **112, part 2**.
12. Candanedo, L.M., W. Obrien, and A.K. Athienitis. *Development of an air-based open loop building-integrated photovoltaic/thermal system model*. in *Building Simulation 2009*. 2009. University of Strathclyde, Glasgow.

13. Eicker, U., V. Fux, D. Infield, L. Mei, and K. Vollmer. *Thermal Performance of building integrated ventilated PV facades*. in *Proceedings of International Solar Energy Conference, Jerusalem* 1999.
14. Bazilian, M.D. and D. Prasad, *Modelling of a photovoltaic heat recovery system and its role in a design decision support tool for building professionals.* Renewable Energy 27, 2002: p. 57-68.
15. Bloem, J.J., *A TRNSYS type calculation model for double skin photovoltaic facades.* Proc. 19th European Photovoltaic Solar Energy Conference and Exhibition, Paris, France, 2004, 2004.
16. Charron, R. and A.K. Athienitis, *A two dimensional model of a double facade with integrated photovoltaic panels.* Journal of Solar Energy Engineering, ASME, 2006. **128**: p. 160-167.
17. Mittelman, G., A. Alshare, and J.H. Davidson, *A model and heat transfer correlation for rooftop integrated photovoltaics with a passive air cooling channel.* Solar Energy, 2009. **In Press, Corrected Proof**.
18. Brinkworth, B.J., R.H. Marshall, and Z. Ibarahim, *A validated model of naturally ventilated PV cladding.* Solar Energy, 2000. **69**: p. 67-81.
19. Brinkworth, B.J. and M. Sandberg, *A validated procedure for determining the buoyancy induced flow in ducts.* Building Service Engineering Research and Technology 2005. **26**(35): p. 35-48.
20. Cipriano, J., C. Lodi, D. Chemisana, G. Houzeaux, and O. Perpinan. *Development and characterization of semitransparent double skin PV facades*. in *EuroSun 2008*. 2008. Lisbon, Portugal.
21. Bazilian, M., N.K. Groenhout, and D. Prasad. *Simplified numerical modelling and simulation of a photovoltaic heat recovery system*. in *17th European photovoltaic solar energy conference*. 2001. Munich, Germany.
22. Cengel, Y., *Heat Transfer: A practical approach*, ed. McGraw-Hill. 1998, New York.
23. Kakac, S., R.K. Shah, and W. Aung, *Handbook of single-phase convective heat transfer*. 1st ed, ed. John Wiley & Sons. 1987.
24. Eicker, U., *Solar technologies for buildings*. First ed, ed. John Wiley. 2003, West Sussex.
25. Tan, H.M. and W.W.S. Charters, *An experimental investigation of forced convective heat transfer for fully developed turbulent flow in a rectangular duct with asymetric heating.* Solar Energy, 1970.
26. Altfeld, K., *Exergetische Optimierung flacher solarer Lufterhitzer*, ed. VDI Verlag. 1985: VDI Verlag.
27. Shah, R.K. and A.L. London, *Laminar flow forced convection in ducts*. 1st ed. Advances in Heat Transfer, ed. Jr. and James P. Harnett Thomas F. Irvine. 1978, New York: Academic Press. 477.
28. Gnielinski, V., *Forced convection in ducts*. Heat exchanger design handbook. , ed. U. Schlunder. Vol. 2. 1983, New York: Hemisphere Publishing Corporation.
29. Chen, Y., A.K. Athienitis, B. Berneche, and P. Y. *Design and simulation of a building integrated photovoltaic thermal system and thermal storage for a solar home.* in *2nd Canadian Solar Buildings Conference*. 2007. Calgary.

30. Kreith, F. and M.B. Bohn, *Principles of Heat Transfer*. 6th ed, ed. Brooks/Cole. 2001, Pacific Grove, CA.
31. Candanedo, J.A., S. Pogharian, A.K. Athienitis, and A. Fry, *Design and simulation of a net zero energy healthy home in Montreal.* 2nd Canadian Solar Buildings Conference, 2007. **1**: p. 1-8.
32. Lienhard, J.H.I. and J.H.V. Lienhard, *A heat transfer textbook*. 3rd ed. 2008, Cambridge, MA: Phlogiston Press.
33. Sopian, K., K.S. Yigit, H.T. Liu, S. Kakac, and T.N. Veziroglu, *Performance Analysis of photovoltaic thermal air heaters.* Energy Conversion and Management, 1996. **37**(11): p. 1657-1670.
34. Garg, H.P. and R.S. Adhikari, *Conventional hybrid photovoltaic/thermal (PV/T) air heating collectors: steady-state simulation.* Renewable Energy, 1997. **11**(3): p. 363-385.
35. Hegazy, A.A., *Comparative study of the performance of four photovoltaic/thermal solar air collectors.* Energy Conversion & Management, 2000. **41**: p. 861-881.
36. Altfeld, K., W. Leiner, and M. Fiebig, *Second Law optimization of flat plate solar air heaters. Part 1: the concept of net exergy flow and the modeling of solar air heaters.* Solar Energy, 1988. **41**(2): p. 127-32.
37. Ong, K.S., *Thermal performance of solar air heaters experimental correlation.* Solar Energy, 1995. **55**: p. 209-220.
38. Ito, S., M. Kashima, and N. Miura, *Flow control and unsteady-state analysis on thermal performance of solar air collectors.* Journal of Solar Energy Engineering, ASME, 2006. **128**: p. 354-359.
39. Dittus, F.W. and L.M.K. Boelter, *Heat transfer in automobile radiators of the tubular type.* International Communications in Heat and Mass Transfer, 1985. **12**(1): p. 3-22.
40. Dittus, F.W. and L.M.K. Boelter, *Heat transfer in automobile radiators of the tubular type.* University of California Publications, 1930. **2**(13): p. 443-461.
41. McAdams, W.H., *Heat Transmission*. 3rd ed. Series in Chemical Engineering, ed. McGraw-Hill. 1954: McGraw-Hill. 532.
42. Martinelli, R.C., *Heat transfer to Molten Metals.* Transactions ASME, 1947. **69**: p. 947-959.
43. Kakac, S. and Y. Yener, *Convective Heat Transfer*. 2nd ed. Vol. 1. 1995, Boca Raton, Florida: CRC Press. 422.
44. Tan, H.M. and W.W.S. Charters, *Effect of thermal entrance region on turbulent forced convective heat transfer for an asymmetrically heated rectangular duct with uniform heat flux.* Solar Energy, 1969. **12**: p. 513-516.
45. Sparrow, E.M., J.R. Lloyd, and C.W. Hixon, *Experiments on Turbulent heat transfer in an asymmetrically heated rectangular duct.* Journal of Heat Transfer. Transactions of the ASME., 1966. **88**: p. 170-174.
46. Novotny, J.L., S.T. McComas, E.M. Sparrow, and E.R.G. Eckert, *Heat transfer for turbulent flow in rectangular ducts with two heated and two unheated walls.* A.I.Ch.E. journal, 1964. **10**(44): p. 466-470.

47. Cheng, K.C. and S.W. Hong, *Effect of tube inclination on laminar convection in uniformly heated tubes for flat-plate solar collectors.* Solar Energy, 1972. **13**: p. 363-371.
48. Malik, M.A.S. and F.H. Buelow. *Heat transfer characteristics of a solar drier*. in *Sun Service Mankind*. 1973. Paris.
49. Metais, B. and E.R.G. Eckert, *Forced, mixed and free convection regimes.* Journal of Heat Transfer, 1964: p. 295-296.
50. Petukhov, B.S., *Turbulent flow and heat transfer in pipes under considerable effect of thermogravitational forces*, in *Heat transfer and turbulent buoyant convection*, D.B. Spalding and N Afgan, Editors. 1976, Hemisphere Publishing Corporation: Washington. p. 701-717.
51. Jackson, T.W., W.B. Harrison, and W.C. Boteler, *Combined Free and forced convection in a constant temperature vertical tube.* Transactions ASME, 1958. **80**: p. 739-745.
52. Brown, C.K. and W.H. Gauvin, *Combined free and forced convection: 1. Heat transfer in aiding flow.* The Canadian journal of Chemical Engineering., 1965. **1**: p. 306-312.
53. Hallman, T.M., *Experimental study of combined forced and laminar convection in a vertical tube.* , in *TN D-1104*, NASA, Editor. 1961, Lewis Research Center: Cleveland, Ohio. p. 44.
54. Brown, W.G., VDI-Forschungsh, 1960. **26**: p. 32.
55. Hausen, H., Wärmetech, 1959. **9**: p. 75-79.
56. Axcell, B.P. and W.B. Hall. *Mixed convection to air in a vertical pipe.* in *Proce. 6th Int. Heat Transfer Conference*. 1978. Toronto, Canada.
57. Fewster, J. and J.D. Jackson. *Enhancement of turbulent heat transfer due to buoyancy for downward flow of water in vertical tubes.* in *Proc. Seminar on Turbulent Buoyant convection*. 1976. Beograd.
58. Osborne, D.G. and F.P. Incropera, *Laminar, mixed convection heat transfer for flow between horizontal parallel plates with asymmetric heating.* International Journal of Heat and Mass Transfer, 1985. **28**(1): p. 207-217.
59. Jackson, J.D., M.A. Cotton, and B.P. Axcell, *Studies of mixed convection in vertical tubes.* International Journal of Heat and Fluid Flow, 1989. **10**: p. 2-15.
60. Aicher, T. and H. Martin, *New correlations for mixed turbulent natural and forced convection heat transfer in vertical tubes.* International Journal of Heat Mass Transfer, 1997. **40**(15): p. 3617-3626.
61. Sudo, Y., M. Kaminaga, and K. Minazoe, *Experimental study on the effects of channel gap size on mixed convection heat transfer characteristics in vertical rectangular channels heated from both sides.* Nuclear Engineering and Design, 1990. **120**(2-3): p. 135-146.
62. Zhang, X. and S. Dutta, *Heat transfer analysis of buoyancy-assisted mixed convection with asymmetric heating conditions.* International Journal of Heat and Mass Transfer, 1998. **41**(21): p. 3255-3264.
63. Dutta, S., X. Zhang, J.A. Khan, and D. Bell, *Adverse and favorable mixed convection heat transfer in a two-side heated square channel.* Experimental Thermal and Fluid Science, 1998. **18**(4): p. 314-322.

64. ASHRAE, *ASHRAE Handbook Fundamentals*, ed. 1791 Tullie Circle. 2005, N.E., Atlanta.
65. Churchill, S.W., *Friction-factor equation spans all fluid flow regimes.* Chemical engineering progress, 1977. **44**(81): p. 91-92.
66. Winterton, R.H.S., *Where did the Dittus and Boelter equation come from?* International Journal of Heat and Mass Transfer, 1998. **41**(4-5): p. 809-810.
67. Kakac, S., *Transient turbulent flow in ducts.* Wärme- und Stoffübertragung, 1968. **1**: p. 169-176.
68. Hatton, A.P. and A. Quarmby, *The effect of axially varying and unsymmetrical boundary conditions on heat transfer with turbulent flow between parallel plates.* International Journal of Heat and Mass Transfer, 1963. **6**: p. 903-914.
69. Kays, W., M. Crawford, and B. Weigand, *Convective heat and mass transfer*. 4th Edition ed. 2005: McGraw Hill. 546.
70. White, F.M., *Fluid Mechanics*. Fifth ed. Series in Mechanical Engineering. 2003: McGraw-Hill. 866.
71. Parametric Technology Corporation, *Mathcad 14*. 2007: Needham, MA.
72. Barrow, H., *An analytical and experimental study of turbulent gas flow between two smooth parallel walls with unequal heat fluxes.* International Journal of heat and mass transfer, 1962. **5**: p. 469-487.
73. Andraos, J., *On the propagation of statistical errors for a function of several variables.* Journal of chemical education 1996. **73**(2): p. 150-154.
74. Taylor, J.R., *An introduction to error analysis*. University Science Books, ed. Calif Sausalito. 1997.
75. McQuiston, F.C., J.D. Parker, and J.D. Spitler, *Heating, Ventilating, and Air Conditioning*. Sixth ed, ed. John Wiley & Sons Inc. 2005.
76. White, F.M., *Viscous Fluid Flow*. Third Edition ed. 2006: McGraw-Hill International Edition.